*inorganics*

MDPI

*Article*

# Copper(II) Bromide Complexes: Crystal Structures, Magnetic Properties, and Hydrogen-Bond-Mediated Exchange

**Žan Zakošek [1,2,*], Evgeny Goreshnik [1], Zvonko Jagličić [3] and Srečo Škapin [4]**

[1] Department of Inorganic Chemistry and Technology, "Jožef Stefan" Institute, Jamova Cesta 39, 1000 Ljubljana, Slovenia; evgeny.goreshnik@ijs.si
[2] Jozef Stefan International Postgraduate School, Jamova Cesta 39, 1000 Ljubljana, Slovenia
[3] Institute of Mathematics, Physics and Mechanics, Faculty of Civil and Geodetic Engineering, University of Ljubljana, Jamova 2, 1000 Ljubljana, Slovenia; zvonko.jaglicic@imfm.si
[4] Advanced Materials Department, "Jožef Stefan" Institute, Jamova Cesta 39, 1000 Ljubljana, Slovenia; sreco.skapin@ijs.si
* Correspondence: zan.zakosek@ijs.si

**Abstract**

Copper(II) compounds exhibit interesting magnetic properties due to halide–halide, copper–halide, and intermolecular hydrogen bond interactions. In this study, seven new copper(II) bromide complexes were synthesised, six of which contain *Dabco* (1,4-diazabicyclo[2.2.2]octane) as a ligand. Single-crystal X-ray diffraction data were refined using both conventional spherical-atom models and a non-spherical-atom approach implemented in NoSpherA2. Magnetic properties were investigated by temperature-dependent magnetic susceptibility and field-dependent magnetisation measurements, analysed using a molecular field approximation. Crystallographic analysis shows that NoSpherA2 significantly improves the description of hydrogen atom positions, yielding C–H and N–H bond lengths closer to neutron diffraction values than conventional refinement. Magnetic measurements indicate that interactions between mononuclear copper(II) centres are determined primarily by the nature of intermolecular exchange pathways rather than copper–copper separations alone. Despite comparable Cu···Cu distances, complexes lacking N–H···Br hydrogen bonds exhibit only weak antiferromagnetic interactions, whereas stronger coupling, effective up to 150 K, is observed when such hydrogen bonds connect neighbouring complexes. These results highlight the importance of hydrogen-bond topology and three-dimensional connectivity in governing magnetic behaviour in mononuclear copper(II) systems.

**Keywords:** copper(II) complexes; non-spherical atom refinement; hydrogen bond-mediated magnetic exchange



Academic Editor: Wolfgang Linert

Received: 20 January 2026
Revised: 2 February 2026
Accepted: 8 February 2026
Published: 11 February 2026



## 1. Introduction

Copper(II) complexes have attracted significant scientific interest due to their structural diversity and rich magnetic behaviour. Owing to their $d^9$ electronic configuration, isolated copper(II) centres are well known to exhibit paramagnetism [1–5]; however, in polynuclear copper(II) species, the close proximity of multiple metal centres enables spin–spin interactions that can significantly alter the magnetic properties of the compounds [1,3,6–9]. Notably, even systems composed exclusively of mononuclear copper(II) complexes, lacking direct copper–copper bonds, may display ferromagnetic or antiferromagnetic behaviour [5,10–12]. Such magnetic coupling can arise from non-covalent intermolecular

interactions, including halide–halide [13–15], copper–halide intermolecular contacts, and hydrogen bonding [16–20], which provide effective exchange pathways between magnetic centres. Density functional theory (DFT) calculations are widely used to complement experimental magnetic data and to rationalise observed magnetic behaviour by elucidating the roles of specific halide–halide and hydrogen-bond-mediated interactions [10,17,20–22]. Calculations on copper(II) monomers show that the magnetic exchange interaction is governed primarily by direct through-space overlap between the orbitals of the donor and acceptor atoms involved in the hydrogen bond (for example, the two oxygen atoms in an O–H···O interaction), while the hydrogen bond itself serves a structural role by keeping these atoms in close proximity [17,22]. For N–H···X interactions (X = Cl, Br), DFT calculations indicate that the larger, and therefore more diffuse and polarisable, $Br^-$ orbitals enhance the antiferromagnetic exchange between mononuclear copper(II) complexes compared to $Cl^-$ [10]. Spin population analysis further confirms that delocalisation of spin density is more pronounced in the presence of larger halide ions [10]. In addition, mononuclear copper(II) complexes have recently been shown to exhibit long spin coherence times at elevated temperatures, making them promising candidates for quantum information processing applications [23].

In the context of copper(II) halide systems, the polyamine ligand 1,4-diazabicyclo[2.2.2] octane (*Dabco*) is an especially attractive building block because it can act as a bridging ligand [24–26], a terminal ligand [24,27,28], or a charge-balancing counterion [29–32], in addition to forming hydrogen bonds that link building blocks [28–30,32]. Despite this versatility, copper–bromide–*Dabco* compounds are surprisingly rare. A survey of the Cambridge Structural Database (CSD, version 6.01, November 2025) reveals only seven reported copper–bromide–*Dabco* crystal structures, six of which are copper(I) species. To date, only one structure (refcode ULAVAF) has been reported for a copper(II)–bromide–*Dabco* compound [32], with $H_2Dabco^{2+}$ acting as a counter-ion and forming hydrogen bonds with $CuBr_4^{2-}$. Given the wide range of coordination numbers and geometries available to copper(II) centres, further investigation of copper(II)–bromide–*Dabco* systems is highly desirable to deepen understanding of structure–property relationships and to enable the rational design of materials with tailored magnetic and functional properties.

We report the synthesis and characterisation of new compounds in the copper–bromide–*Dabco* system. Their crystal structures were refined using a modern non-spherical-atom refinement method, and their magnetic properties were investigated.

## 2. Results and Discussion

### *2.1. Structural Analysis*

#### 2.1.1. Compound **1**, H*Dabco*$CuBr_3H_2O$

Compound **1** crystallises in the orthorhombic space group $Pna2_1$. As shown in Figure 1, the geometry of the $Cu^{2+}$ centre is a slightly distorted trigonal bipyramid, with $\tau_5$ equal to 0.81, where $\tau_5 = 0$ describes a perfect square pyramidal geometry and $\tau_5 = 1$ a perfect trigonal bipyramidal geometry [33]. All three $Br^-$ ions occupy the equatorial plane, while the water molecule and the H*Dabco* molecule are in the axial positions.

Each complex is connected to four neighbouring complexes through hydrogen bonds. Three of these originate from the water molecule and one from the H*Dabco* molecule (Figure 2), with distances from O1 to $N2^{i}$, $Br2^{ii}$, and $Br3^{iii}$ being 2.969(5), 3.257(3), and 3.296(3) Å, respectively.

#### 2.1.2. Compound **2**, H*Dabco*$CuBr_3$*Dabco*

Compound **2** crystallises in the *R*32 space group, and its asymmetric unit contains one $Cu^{2+}$ ion, one $Br^-$ ion, and one third of a *Dabco* molecule. The complete complex of

compound **2** has the formula H*Dabco*CuBr$_3$*Dabco*, with the copper(II) centre coordinated by three equatorial Br$^-$ ions and two axial *Dabco* molecules. The parameter $\tau_5$ is 1.0, as the copper(II) centre lies at the intersection of the threefold and twofold axes. As shown in Figure 3, complexes of compound **2** are connected through hydrogen bonds via N2 atoms (d(N2···N2$^{i}$) = 2.648(10) Å). The H2 atom attached to N2 was placed using the AFIX 13 command, and its occupancy was set to 0.50 relative to N2, as two hydrogen atoms cannot be present at this distance simultaneously.

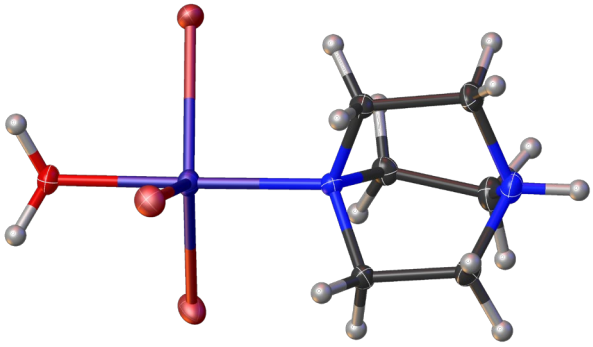

**Figure 1.** The copper(II) centre displays a trigonal bipyramidal coordination geometry in compound **1**.

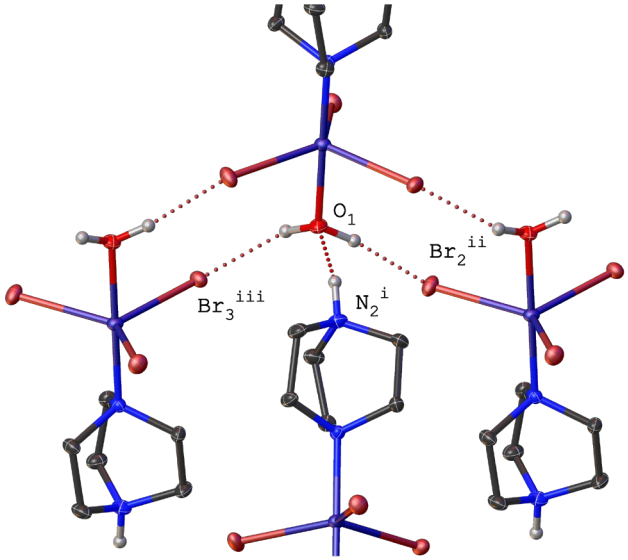


**Figure 2.** Hydrogen-bond system in compound **1** (viewed along the [010] crystallographic direction). Hydrogen atoms bonded to carbon atoms are omitted for clarity. Symmetry operations: (i) –1/2 + X, 1/2–Y, +Z; (ii) 1–X, 1–Y, –1/2 + Z; (iii) 1–X, 1–Y, 1/2 + Z.

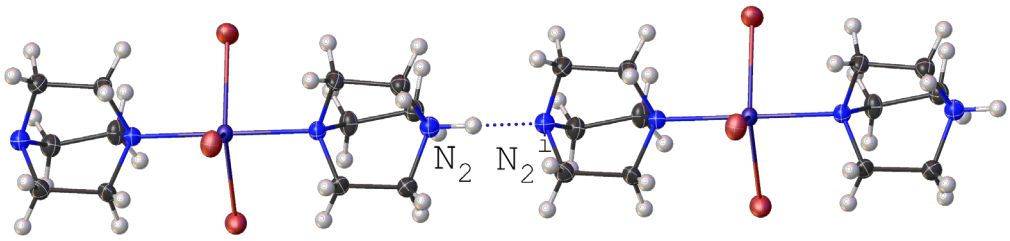


**Figure 3.** Representation of hydrogen bonds between complexes in compound **2** (viewed along the [100] crystallographic direction). Symmetry operation: (i) 1/3–Y + X, 2/3–Y, 2/3–Z.

Complexes of compound **2** are aligned along the [001] direction, forming a chain-like structure (Figure 4), in which individual complexes are connected by hydrogen bonds. There are no hydrogen or halogen bonds between the chains.

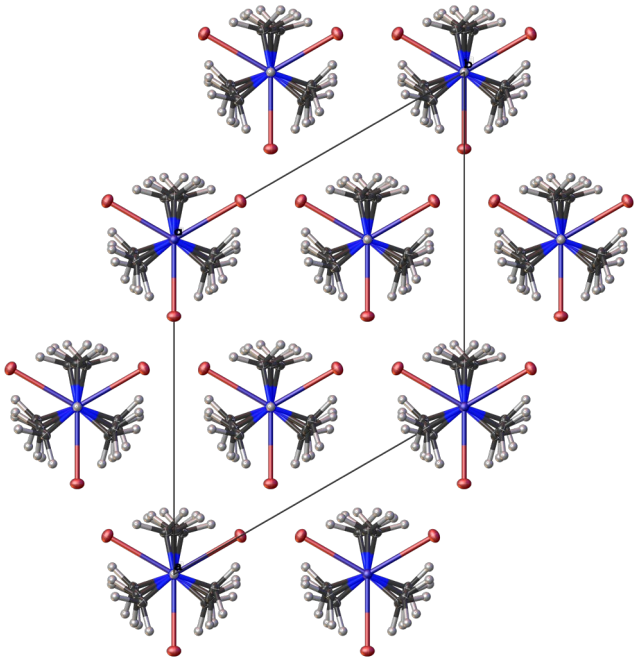

**Figure 4.** Packing of the unit cell viewed along the [001] crystallographic direction. The chain-like structure extends along the [001] direction. There are no hydrogen bonds between complexes in different chains.

#### 2.1.3. Compound **3**, $[(H\textit{Dabco})_2CuBr_3]Br$

The complex present in compound **3** is very similar to the H*Dabco*$CuBr_3$*Dabco* complex found in compound **2**, with the only difference being that both *Dabco* molecules are protonated. As both *Dabco* molecules are protonated, there is one additional $Br^-$ ion in the structure, which connects two $[(H\textit{Dabco})_2CuBr_3]^+$ complexes via hydrogen bonds (d(Br3···N2) = 3.124(4) Å and d(Br3···$N4^i$) = 3.210(4) Å), forming a chain-like structure along the 001 direction, as shown in Figure 5. The geometry of the $Cu^{2+}$ centre is again a slightly distorted trigonal bipyramid, with $\tau_5$ equal to 0.75.

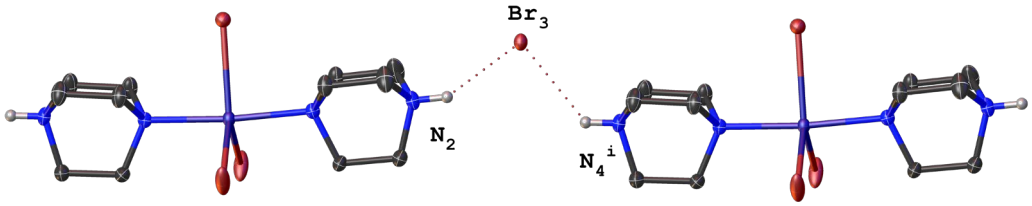


**Figure 5.** Representation of hydrogen bond connections between two $[(H\textit{Dabco})_2CuBr_3]^+$ complexes via a free $Br^-$ ion in compound **3** (viewed along the [010] crystallographic direction). Hydrogen atoms bonded to carbon atoms are omitted for clarity. Symmetry operation: (i) + X, 1/2–Y, 1 + Z.

#### 2.1.4. Compound **4**, $[CuBr_2(\mu\textit{-Dabco})ACN]_n$

Compound **4** consists of chains with the unit formula $[CuBr_2(\mu\textit{-Dabco})ACN]_n$ running along the [100] direction (Figure 6). *Dabco* acts as a bridging ligand, connecting two copper(II) centres. The geometry of the $Cu^{2+}$ centre is a distorted trigonal bipyramid, with $\tau_5$ = 0.74.

There are no hydrogen or halogen bonds between the 1D chains (Figure 7). The orientation of ACN alternates between each of the 1D chains.

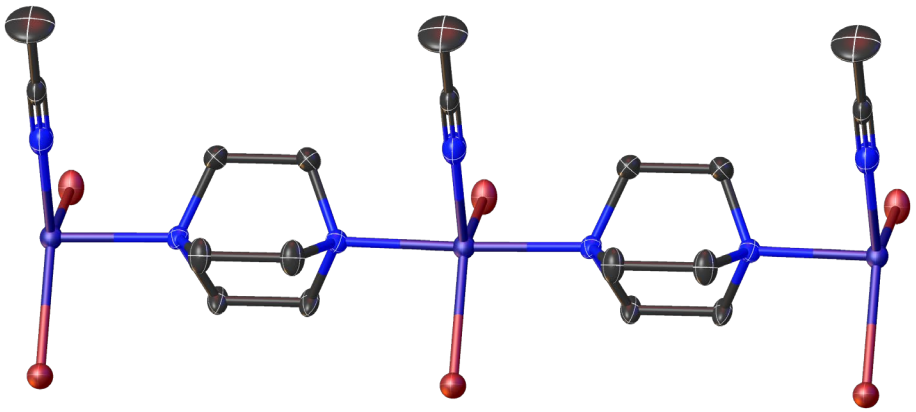

**Figure 6.** View along the [011] crystallographic direction of the 1D chain with the formula [CuBr*Dabco*ACN], present in compound **4**. Hydrogen atoms are omitted for clarity.

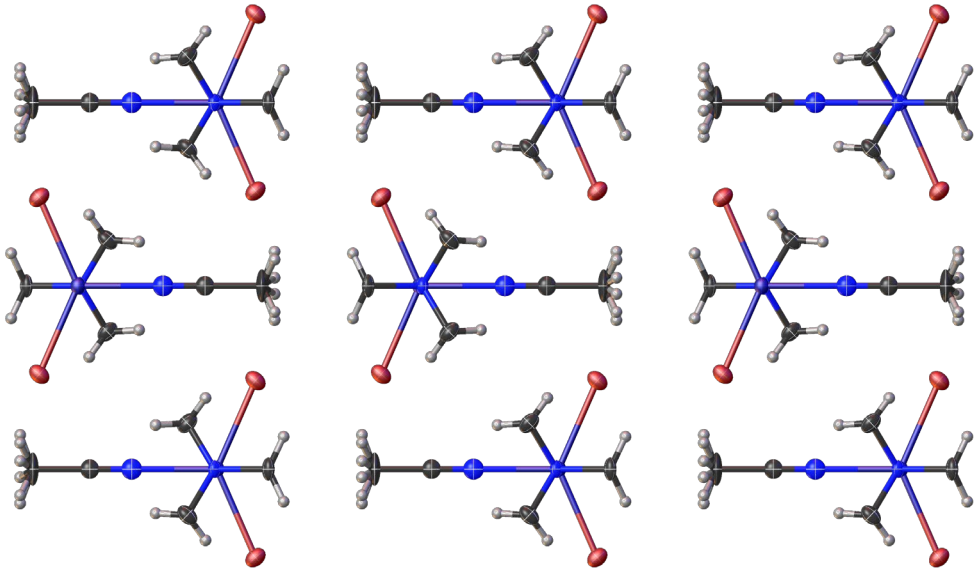

**Figure 7.** Packing of compound **4** showing the alternating orientation of the ACN molecule between chains, viewed along the [100] crystallographic direction.

#### 2.1.5. Compound **5**, $(H_2Dabco)Cu_2Br_6$

In compound **5**, within the inorganic anion $[Cu_2Br_6]^{2-}$, the distances between Cu1 and Br atoms are significantly shorter (2.4061(7), 2.4261(7), 2.4597(7) and 2.4799(7) Å for Br3, Br2, Br1, and $Br1^i$, respectively) than the distance of 2.7695(8) Å between Cu1 and $Br3^i$. Although this latter distance is still significantly shorter than the sum of the van der Waals radii (2.38 and 1.86 Å for copper and bromine atoms, respectively) [34], it is greater than the sum of the covalent radii of copper and bromine atoms (1.35 and 1.15 Å, respectively) [35]; thus, this bond can be described as semi-coordinate. As shown in Figure 8, the $[Cu_2Br_6]^{2-}$ anions are connected by semi-coordinated Cu–Br bonds and by hydrogen bonds through $H_2Dabco^{2+}$ molecules (d(Br2···N1) = 3.21732(10) Å). The $\tau_4$ parameter for Cu1 is 0.23, which suggests a strongly distorted square planar configuration. However, if $Br3^i$ is taken into account, the geometry of each $Cu^{2+}$ metal centre is a strongly distorted square pyramid, with $\tau_5$ = 0.38. The structure is isostructural with the chloride analogue published in the CSD under the refcode ICAZIZ [31]. Distances in the reported $[Cu_2Cl_6]^{2-}$ anion between copper and chloride atoms range from 2.263 to 2.331 Å, while the distance to the semi-coordinated chlorine atom is 2.660 Å. In the original paper, only $\tau_5$ was reported, with a value of 0.39, which is similar to the 0.38 of the bromide analogue reported in our paper [31].

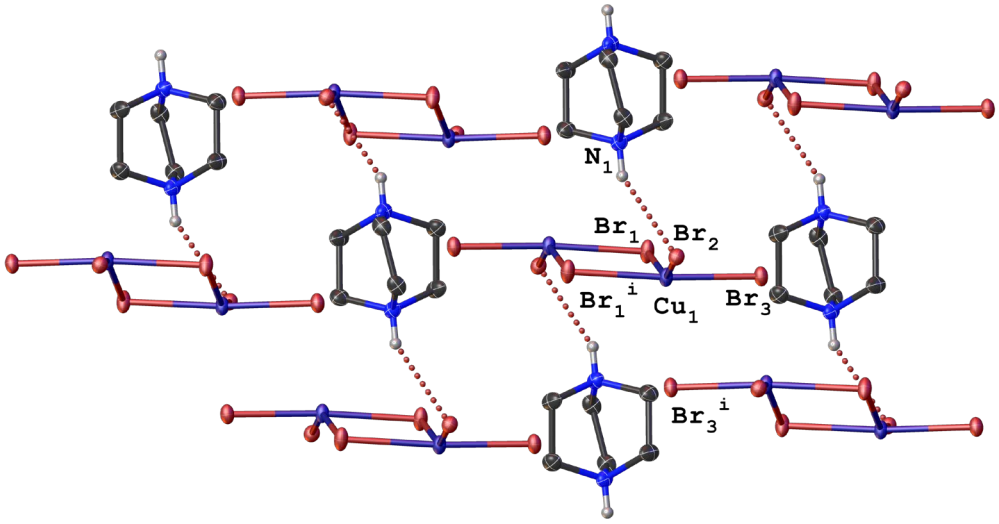


**Figure 8.** The $H_2$*Dabco*$^{2+}$ molecules serve as linkers between the $[Cu_2Br_6]^{2-}$ anions in compound **5**, as viewed along the [010] crystallographic direction. The distance of 2.7695(8) Å between Cu1 and Br3$^{i}$ exceeds than the sum of the covalent radii of copper and bromine atoms. Hydrogen atoms bonded to carbon atoms are omitted for clarity. Symmetry operation: (i) 3/2–X, +Y, 1/2–Z.

### 2.1.6. Compound **6**, $(C_2N_2H_7)_2[Cu_2Br_2(CH_3COO)_4]$

In compound **6**, binuclear copper(II) paddle-wheel complexes and amidinium cations are present (Figure 9). The $[Cu_2Br_2(CH_3COO)_4]^{2-}$ paddle-wheel complex has two $Br^-$ ions at the apical positions and shows a weak copper–copper interaction, with a Cu–Cu distance of 2.6379(6) Å.

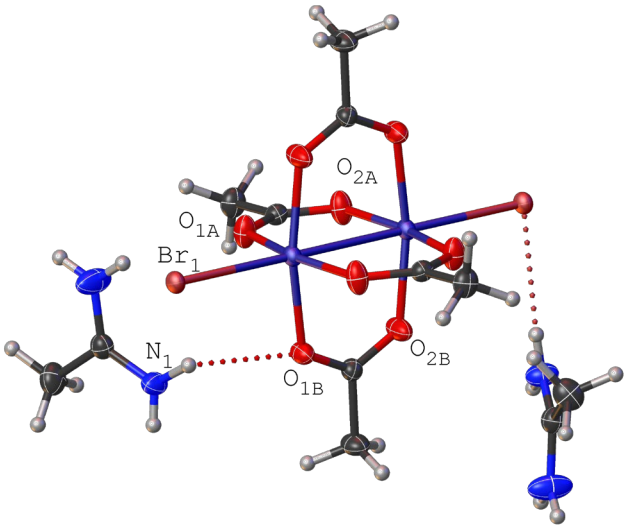


**Figure 9.** Compound **6** contains a copper(II) acetate paddle-wheel with $Br^-$ ions at the apical positions, and amidinium cations act as counter-ions.

The paddle-wheels (Figure 10) are linked by hydrogen bonds through O1B and Br1 to the amidinium cation, where only N1 forms hydrogen bonds (d(N1···O1B) = 3.09585(5) Å, d(N1···Br1$^{i}$) = 3.39300(8) Å).

### 2.1.7. Compound **7**, H*Dabco*$CuBr_3$

In contrast to the previous compounds in this article, the copper(II) centre in compound **7** has a coordination number of 4 (Figure 11). Three $Br^-$ ions and one protonated *Dabco* are attached to the copper centre. The $\tau_4$ parameter, where $\tau_4 = 0$ indicates a

perfectly square planar geometry and $\tau_4 = 1$ indicates a perfectly tetrahedral geometry [36], is 0.82 for this compound, indicating a distorted tetrahedral coordination geometry, which is more common in complexes with copper in the +1-oxidation state.

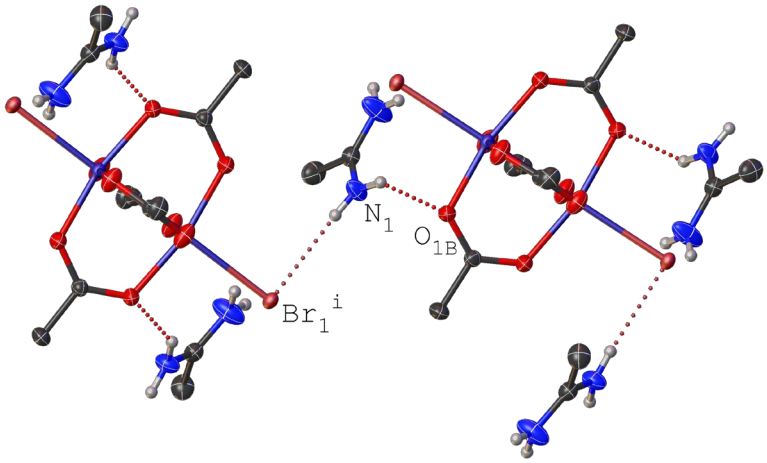


**Figure 10.** Amidinium cations link copper acetate paddle-wheel complexes via hydrogen bonds between N1 and Br1$^{i}$, and between N1 and O1B in compound **6**. Symmetry operation: (i) –1/2 + X, 1/2–Y, 1/2 + Z. Hydrogen atoms bonded to carbon atoms are omitted for clarity.

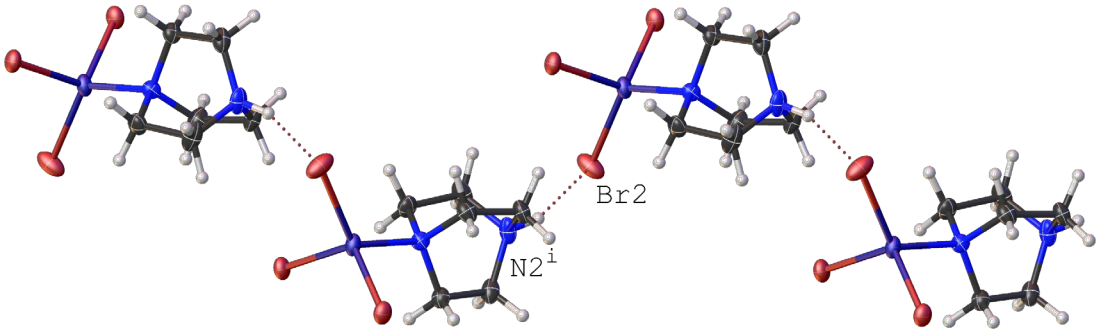


**Figure 11.** Hydrogen bonds exist between [HDabco]CuBr3 complexes in compound **7**. The hydrogen bond network extends along the b axis, with 3.411(7) Å between N2$^{i}$ and Br2. Symmetry operation: (i) 1–X, 1/2 + Y, 2–Z.

Neighbouring complexes are connected by hydrogen bonds running in the [010] crystallographic direction, with bond distances between N2 and Br2$^{i}$ of 3.411(7) Å.

#### 2.1.8. Different Roles and States of the *Dabco* Molecule in Structures

As shown by compounds **1** to **5** and **7**, organic polyamine ligands such as *Dabco* can exist in various forms (unprotonated, mono- or deprotonated, or any combination of these three states, as in compound **2**). They can also act as bridging ligands (compound **4**), terminal ligands (compound **7**), or as uncoordinated free cations within the structure (compound **5**). This wide range of possibilities, combined with the different coordination numbers (**4** or **5**) of copper(II) centres and the possibility of $Br^{-}$ acting as a bridging ligand (compound **5**), leads to the formation of many different copper–halide–polyamine complexes with varying properties.

### *2.2. Hirshfeld Atom Refinement Using NoSpherA2*

Tables 1 and 2 compare refinement parameters after the Independent Atom Model (IAM) and Hirshfeld Atom Refinement (HAR).

**Table 1.** Summary of IAM and HAR refinements for structures **1**–**3**.

| **Compound** | **1** | **2** | **3** |
|---|---|---|---|
| Formula for HAR | [H*Dabco* $CuBr_3H_2O]_4$ | [H*Dabco*$CuBr_3$*Dabco*]$_2$ | ([(H*Dabco*)$_2$$CuBr_3$]Br)$_2$ |
| Resolution Å | 0.79 | 0.81 | 0.79 |
| I/σ | 30.0 | 59.9 | 52.1 |
| Number of parameters IAM/HAR | 130/254 | 32/50 | 118/166 |
| Charge, multiplicity | 0, 5 | 0, 3 | 0, 3 |
| R1 (IAM)/% | 2.47 | 1.77 | 3.15 |
| R1 (HAR)/% | 2.36 | 1.58 | 2.88 |
| Δ$\rho$ (IAM)/ eÅ$^{-3}$ | −0.458, 0.668 | −0.271, 0.376 | −0.458, 0.772 |
| Δ$\rho$ (HAR)/ eÅ$^{-3}$ | −0.4100, 0.5929 | −0.2615, 0.4125 | −0.5334, 0.9534 |

**Table 2.** Summary of IAM and HAR refinements for structures **4**–**7**.

| **Compound** | **4** | **5** | **6** | **7** |
|---|---|---|---|---|
| Formula for HAR | [CuBr*Dabco*ACN] | $H_2$*Dabco*$Cu_2Br_6$ | $(C_2N_2H_7)_6$ $[Cu_2Br_2(CH_3COO)_4]_3$ | (H*Dabco*$CuBr_3$)$_2$ |
| Resolution Å | 0.79 | 0.81 | 0.79 | 0.80 |
| I/σ | 25.8 | 32.8 | 60.2 | 26.7 |
| Number of parameters IAM/HAR | 45/57 | 76/101 | 146/244 | 113/160 |
| Charge, multiplicity | 0, 2 | 0, 3 | 0, 7 | 0, 3 |
| R1 (IAM)/% | 4.02 | 3.20 | 2.45 | 2.93 |
| R1 (HAR)/% | 3.77 | 3.16 | 2.22 | 2.82 |
| Δ$\rho$ (IAM)/ eÅ$^{-3}$ | −0.618, 1.480 | −0.972, 1.025 | −0.601, 0.478 | −0.542, 0.862 |
| Δ$\rho$ (HAR)/ eÅ$^{-3}$ | −0.6443, 1.6695 | −1.0508, 1.0199 | −0.4208, 0.3757 | −0.6264, 0.8150 |

In all cases, implementing NoSpherA2 refinement reduced the R1 factors. It should be noted that for compound **5**, the change in R1 value is only 0.04%. This structure contains an inorganic one-dimensional chain of copper(II) bromide. We expanded our model to include up to six copper centres, aiming for a better representation of the 1D chain structure for wavefunction calculation. However, expanding the structure to six copper(II) centres yielded results like those obtained with only two centres. For each copper centre, the appropriate number of $Br^-$ and *Dabco* molecules was also included in the wavefunction calculation for compound **5**.

After calculating the non-spherical scattering factors and refining the structures accordingly, we plotted deformation density maps to visualise the changes in the description of electron density by the IAM and HAR models.

In the structure of compound **1** (Figure 12), using the HAR model, lone electron pairs are clearly observed around the oxygen atoms, which participate in the formation of

hydrogen bonds with the surrounding *Dabco* molecules. The HAR model also describes the electron density present in C–H, C–C, and Cu–N bonds, while a depletion of electron density is observed near the heavy atoms (copper and bromine ions).

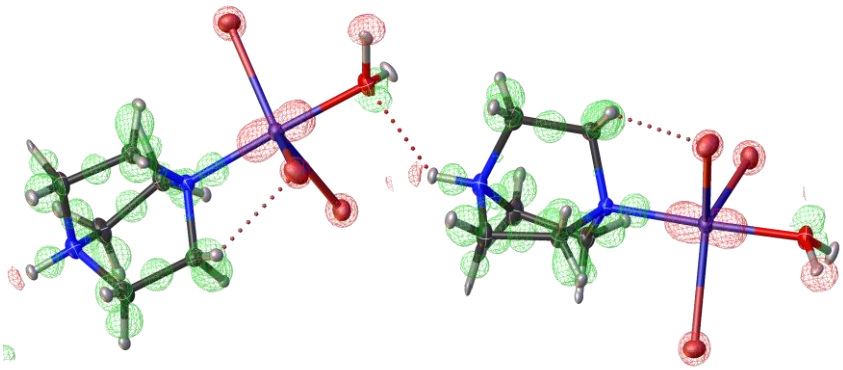

**Figure 12.** Deformation map of the complex in compound **1** (grid = 0.10 Å, iso-value = 0.20 eÅ$^{-3}$). Free electron pairs around oxygen and additional electron density (green) on C–H and C–C bonds, as well as depletion (red) of electron density around Cu and Br atoms can be observed.

A similar depiction of lone pairs is evident in Figure 13 around the nitrogen atoms in compound **2**, confirming the presence of hydrogen bonds between the two complexes of compound **2**.

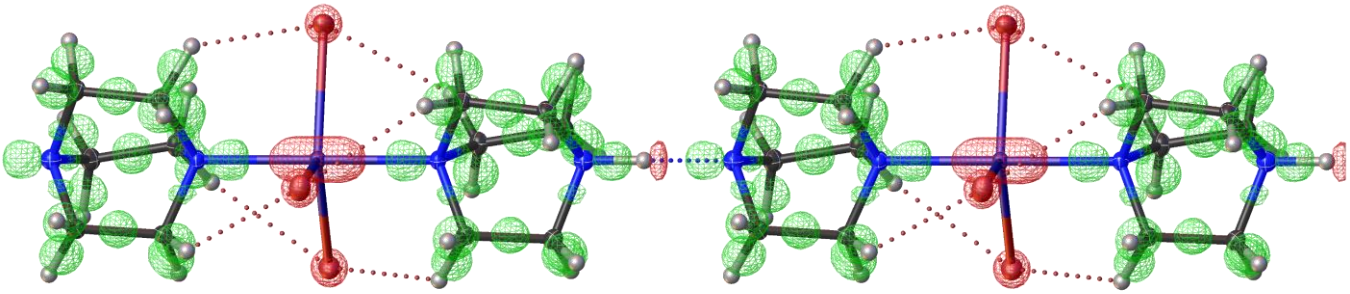

**Figure 13.** The deformation map for compound **2** (grid = 0.10 Å, iso-value = 0.20 eÅ$^{-3}$), using the HAR model, shows free electron pairs around nitrogen atoms and additional electron density (green) on C–H, C–C, C–N, and Cu–N bonds, as well as depletion (red) of electron density around Cu and Br atoms.

Although all data were measured using Kα Cu radiation, for compound **6**, anisotropic refinement of hydrogens is also possible and results in a slight improvement in the R1 factor. In addition to describing lone pairs, the use of non-spherical scattering factors allows the electron density associated with delocalised chemical bonds to be properly described. In contrast, in the IAM, delocalised electron density is not represented. For example, in compound **6** (Figure 14), there is a slight depletion of electron density above and below the carbon atom in the –COO$^-$ group of acetate, which indicates electron delocalisation in the –COO$^-$ group.

### *2.3. Comparison with Neutron Data*

Average distances of C–H and N–H bonds in the *Dabco* molecule for each compound, before and after NoSphereA2 refinement, were compared with neutron data from eight entries in the Cambridge Structural Database (CSD) for *Dabco* molecules. The data are

summarised in Table 3. Refcodes of structures from the CSD, along with bond distances, are provided in the Supplementary Materials (Tables S3 and S4).

$$d_{average} = \frac{\sum_i^N w_i \times d_i}{\sum_i^N w_i} \quad (1)$$

$$\sigma^2 = \frac{N}{N-1} \frac{\sum_i^N w_i \times (d_i - d_{average})^2}{\sum_i^N w_i} \quad (2)$$

$$w_i = \frac{1}{\sigma_i^2}, \text{ where } \sigma_i \text{ is the standard uncertainty of bond } i \quad (3)$$

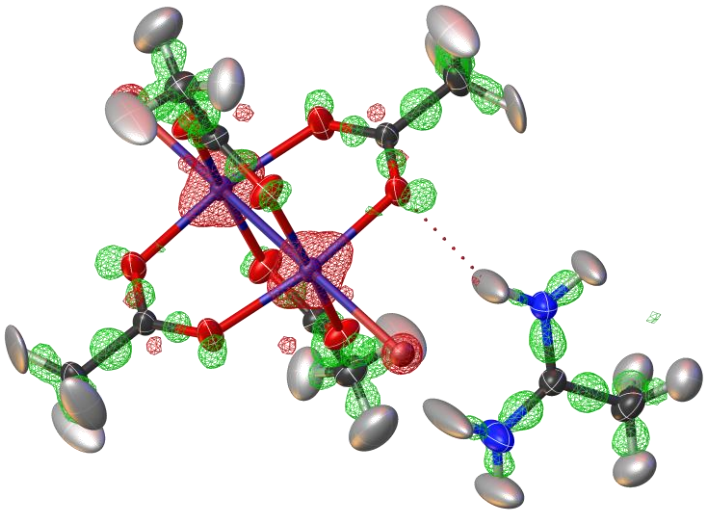

**Figure 14.** The deformation map presented for compound **6** (grid = 0.10 Å, iso-value = 0.20 eÅ$^{-3}$) shows that, using the HAR model, free electron pairs are described around the oxygen atoms of the acetate group, along with additional electron density (green) on C–H, C–C, C–O, C–N and N–H bonds, as well as depletion (red) of electron density due to delocalisation of bonds around the carbon atom in the –COO$^-$ group.

**Table 3.** Comparison of average C–H and N–H distances in individual structures using IAM and HAR refinement with neutron data.

| | **d(C–H) [Å]** | | **d(N–H) [Å]** | |
|---|---|---|---|---|
| CSD neutron data | 1.07(5) | | 1.07(3) | |
| Compound | IAM | HAR | IAM | HAR |
| **1** | 0.99 * | 1.04(7) ** | 0.94(4) | 0.95(5) |
| **2** | 0.99 * | 1.06(5) ** | AFIX 13 | 1.1(1) |
| **3** | 0.99 * | 1.05(6) ** | 0.86(1) ** | 1.02(3) ** |
| **4** | 0.99 * | 1.07(5) ** | No N-H bond | |
| **5** | 0.99 * | 1.11(9) ** | 0.83(8) | 1.02(8) |
| **6** | no *Dabco* molecule | | no *Dabco* molecule | |
| **7** | 0.99 * | 1.10(9) ** | 0.89(11) | 1.02(9) |
| Average | 0.99 | 1.06(7) ** | 0.90(5) ** | 1.00(4) ** |

* Distances come from AFIX 23 command. ** Average bond distances ($d_{average}$) and standard deviations were calculated using formulas.

As shown in Table 3, particularly for the C–H distances, implementing non-spherical refinement increases the C–H and N–H distances. The increased C–H and N–H distances

in *Dabco* molecules are closer to those measured by neutron diffraction. Individual bond distances for each compound, can be found in the Supplementary Materials (Tables S5–S8).

### *2.4. Magnetic Properties*

The magnetic behaviour of the mononuclear copper(II) complexes of compounds **2**, **4**, and **7** is presented in Figure 15. At room temperature, the measured effective magnetic moments are 1.84 $\mu_B$, 1.73 $\mu_B$, and 1.84 $\mu_B$ for complexes **2**, **4**, and **7**, respectively. These values are close to the theoretical spin-only value of 1.73 $\mu_B$ [37], which corresponds to a non-interacting copper(II) ion with spin quantum number $S = 1/2$ and a completely quenched orbital contribution ($L = 0$).

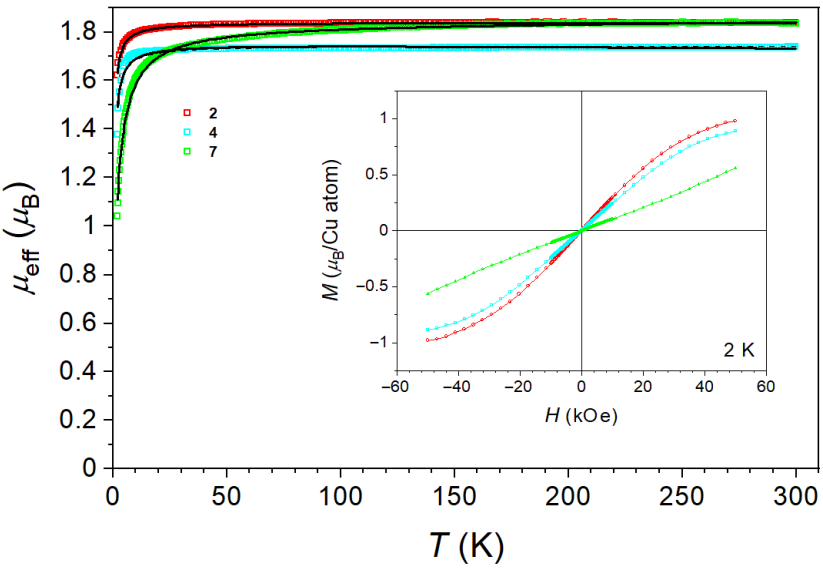


**Figure 15.** The effective magnetic moment $\mu_{eff}$ as a function of temperature for complexes **2**, **4**, and **7**. The solid lines represent fits using a model based on the molecular field approximation. The inset shows the isothermal magnetisation of the three complexes at 2 K.

As the temperature decreases, the effective magnetic moment remains nearly constant down to approximately 150 K for complex **7** and to about 30 K for complexes **2** and **4**. A temperature-independent magnetic moment is characteristic of paramagnetic behaviour. Below 150 K for complex **7**, and below 30 K for complexes **2** and **4**, the effective magnetic moment decreases with further cooling, indicating that antiferromagnetic interactions between the magnetic centres become effective.

The isothermal magnetisation $M(H)$ at 2 K (inset in Figure 15) is consistent with the observed temperature dependence of the effective magnetic moment. For complexes **2** and **4**, the $M(H)$ curves at 2 K exhibit a Brillouin-like shape typical of paramagnetic behaviour, corresponding to the slight decrease in the effective magnetic moment at the lowest temperatures and indicating a weak antiferromagnetic interaction. In contrast, the $M(H)$ curve for complex **7** is almost linear up to the maximum applied field of 50 kOe (equivalent to 5 T), reflecting a much stronger antiferromagnetic interaction between the magnetic centres.

To estimate the magnetic interactions between the magnetic moments, it is first necessary to select an appropriate magnetic model that reflects the spatial arrangement of the copper(II) magnetic moments within the compounds.

In compound **2** (H*Dabco*$CuBr_3$*Dabco*), N–H···N hydrogen bonds are present (d(N···N) = 2.648(10) Å), connecting two complexes with copper centres 12.0726(4) Å apart (translation along the *c* axis). The shortest distance between two copper atoms is 7.48164(13) Å,

occurring between copper atoms in neighbouring chains (Figure 4). There are no hydrogen or halogen bonds between the complexes of these two copper atoms.

In compound **4** ([$CuBr_2$(*μ-Dabco*)ACN]$_n$), a quasi 1D chain structure of Cu(II) ions is formed, where two copper atoms are separated by a single bridging *Dabco* molecule (Figure 6) at a distance of 6.8435(5) Å (translation along the *a* axis). However, the distance to copper centres in neighbouring 1D chains is only slightly larger, at 6.8507(11) Å. There are no halogen or hydrogen bonds between the [$CuBr_2$(*μ-Dabco*)ACN]$_n$ chains.

In compound **7** (H*Dabco*$CuBr_3$), N–H···Br hydrogen bonds connect the tetrahedral complexes, with intermolecular copper–copper distances of 8.2844(13) Å (Figure 11). However, the shortest intermolecular copper–copper distance is 6.8789(8) Å, but there are no hydrogen or halogen bonds between the complexes of these two copper centres.

In all three compounds investigated, the magnetic moments form a three-dimensional network. Even in the quasi-one-dimensional compound **4**, the distances between magnetic centres along the chain are very similar to those between centres in neighbouring chains. This prevents the use of models restricted to low-dimensional magnetism. Therefore, we described the temperature-dependent susceptibility using the molecular field approximation. The freely available software PHI was used to determine the mean-field interaction parameter, *zJ* [38]. The results of the fits are shown as solid lines in Figure 15, and the obtained parameters (*g*-factors and *zJ* for each compound) are summarised in Table 4.

**Table 4.** The fitting parameters were obtained using a mean-field approximation to describe the temperature dependence of magnetic susceptibility.

| Complex | *g*-Factor | *zJ* (cm$^{-1}$) |
|---|---|---|
| **2** | 2.12 | −0.34 |
| **4** | 2.02 | −0.52 |
| **7** | 2.12 | −2.15 |

As expected, the largest interaction parameter was found for compound **7**. The main structural difference between compounds **2** and **4** and compound **7** is the presence of N–H···Br hydrogen bonds: while no N–H···Br hydrogen bonds exist between nearest copper(II) neighbours in **2** and **4**, the tetrahedral copper(II) units in **7** are connected via N–H···Br hydrogen bonds [10,19]. Although magnetic interactions between copper(II) centres connected through X–H···Y (X, Y = N, O) hydrogen bonds are also known [5,16,17,20,22], in compound **2** the distances between nearest copper(II) centres appear too great. It is also worth noting that the rather weak magnetic interaction in compound **4** rules out magnetic coupling mediated solely by the *Dabco* molecule.

## 3. Materials and Methods

### *3.1. Materials*

All experiments were conducted under atmospheric air without special conditions. Copper powder (purity 99.5%), $CuBr_2$ (purity 99%), 1,4-diazabicyclo[2.2.2]octane, and HBr (48% solution in water) were purchased from Sigma-Aldrich. Acetonitrile (ACN) was also purchased from Sigma-Aldrich. Methanol (MeOH) was purchased from Carlo Erba.

The HBr salt of *Dabco* (H*Dabco*Br) was synthesised by combining 2.905 g of *Dabco* with 2.930 mL of HBr in 10 mL of acetonitrile (ACN). The mixture was stirred for 30 min, then the solvent was allowed to evaporate under ambient conditions. Evaporation yielded 4.575 g of the desired salt (H*Dabco*Br).

### *3.2. Single Crystal Preparation*

#### 3.2.1. Compound **1**, H*Dabco*$CuBr_3H_2O$

In a 5 mL test tube, 37 mg of $CuBr_2$, 223 mg of *Dabco*, and 0.104 mL of HBr (aq, 48%) were combined with 4 mL of ACN and mixed thoroughly with a spatula. A copper wire was coiled into a spiral with a diameter of approximately 1 cm, and a second straight copper wire was inserted through the centre of the spiral. Both wires were fixed in a cork, immersed in the reaction mixture, and connected to an alternating current source (50 Hz, 0.7 V). After three days, slightly orange crystals were collected from the bottom of the test tube, along with an orange precipitate.

#### 3.2.2. Compound **2**, H*Dabco*$CuBr_3$Dabco

The same procedure as for compound **1** was used to obtain crystals of compound **2**. In this case, 33 mg of $CuBr_2$, 114 mg of *Dabco*, and 0.113 mL of HBr were used. After 3 days, the test tube was disconnected from the electrical current and placed in the freezer. After 16 days, thin red needles were collected from the wires in the test tube and measured.

#### 3.2.3. Compound **3**, [(H*Dabco*)$_2CuBr_3$]Br

As with compounds **1** and **2**, a similar procedure was followed to obtain crystals of compound **3** (80 mg $CuBr_2$, 86 mg *Dabco*, and 0.104 mL HBr). After 2 days, the test tube was disconnected from the electrical current and placed in the freezer. After 4 days, yellow plates were observed around the copper wire. These were collected from the wire and measured.

#### 3.2.4. Compound **4**, [$CuBr_2$(*μ-Dabco*)ACN]$_n$

Crystals of compound **4** were prepared by mixing 0.32 mg of CuBr, 22 mg of H*Dabco*Br salt, and 12 mg of *Dabco* with 5 mL of ACN in a 7 mL vial. The vial was placed in the ALEMADR-MS Laboratory Dry Block Thermo Shaker Incubator. The following temperature and mixing programme were set: 24 h at 800 rpm and 100 °C, 6 h at 0 rpm and 100 °C, 12 h at 800 rpm and 100 °C, 10 h at 0 rpm and 80 °C, and a final cycle of 10 h at 0 rpm and 60 °C.

#### 3.2.5. Compound **5**, ($H_2$*Dabco*)$Cu_2Br_6$

Following the procedures established for compounds **1–3**, crystals of compound **5** were synthesised by combining 133 mg of $CuBr_2$, 71 mg of *Dabco*, and 0.317 mL of HBr in a test tube. After maintaining the reaction for 3 days under an applied electrical current, the test tube was disconnected from the power source. The tube was then opened and covered with Parafilm perforated with small holes to allow for slow solvent evaporation. After 10 days, the solvent had completely evaporated, yielding black crystalline solids identified as compound **5**.

#### 3.2.6. Compound **6**, $(C_2N_2H_7)_2[Cu_2Br_2(CH_3COO)_4]$

Crystals of compound **6** were obtained by a solvothermal reaction. In a 50 mL Teflon-lined vessel, 450 mg of $CuBr_2$, 60 mg of copper powder, 342 mg of *Dabco*, 1.6 mL of HBr, and 20 mL of ACN were mixed. The autoclave was placed in a preheated oven at 150 °C for 6 days. After slow cooling, the yellow solution was placed in a freezer, and after 1-month, green crystals were collected from the solution.

#### 3.2.7. Compound **7**, H*Dabco*$CuBr_3$

To prepare crystals of compound **7**, 223 mg of CuBr2, 85 mg of *Dabco*, 0.086 mL of HBr, and 10 mL of MeOH were placed in a 20 mL vial and stirred for 96 h. Afterwards, the powder product and solution were separated. The orange solution was transferred to a

separate vial covered with perforated Parafilm to allow the solvent to evaporate slowly over the next three days. The powder obtained was left in the open vial to dry and was used for further analysis.

In each of these experiments (except for compound **7**), crystals of copper(I) bromide and *Dabco* complexes were obtained. Their structures will be published in a separate paper, focusing on the systematic investigation of compounds from the CuBr–HBr–*Dabco* ternary system and their properties.

### *3.3. Powder Sample Preparation*

#### 3.3.1. Compound **2**

To prepare compound **2** for further analysis, 300 mg of CuBr2, 305 mg of *Dabco*, 0.153 mL of HBr, and 20 mL of ACN were placed in a flask and mixed overnight. The solvent was removed, and the sample was dried under reduced pressure. Finally, 630 mg (88.6% yield) of red powder was collected from the flask for further analysis. Measured and simulated powder X-ray data are provided in the Supplementary Materials (Figure S1). Elemental analysis: expected: C 27.27%, H 4.77%, N 10.60%, Cu 12.02%; found: C 27.61%, H 4.99%, N 10.40%, Cu 11.33%.

#### 3.3.2. Compound **4**

To prepare compound **4** for further analysis, 223 mg of $CuBr_2$, 115 mg of *Dabco*, and 40 mL of ACN were placed in a flask and heated at 100 °C for 48 h. Afterwards, the solvent was decanted and the sample was dried under reduced pressure. A total of 118 mg (31.3% yield) of dark red powder was obtained. Measured and simulated powder X-ray data are provided in the Supplementary Materials (Figure S2). Elemental analysis: expected: C 25.52%, H 4.02%, N 11.16%, Cu 16.87%; found: C 25.51%, H 4.27%, N 10.54%, Cu 15.84%.

#### 3.3.3. Compound **7**

To prepare compound **7** for further analysis, the dried powder obtained from the preparation of single crystals of compound **7** (Section 3.2.7) was collected from the vial. A total of 301 mg (94.5% yield) of black powder was obtained. Measured and simulated powder X-ray data are provided in the Supplementary Materials (Figure S3). Elemental analysis: expected: C 17.31%, H 3.15%, N 6.73%, Cu 15.26%; found: C 16.82%, H 3.21%, N 6.32%, Cu 14.89%.

### *3.4. Single Crystal X-Ray Data Measurement and Analysis*

Single-crystal data for compounds **1**–**6** were collected on a Gemini A diffractometer equipped with an Atlas CCD detector, using graphite-monochromated CuKα radiation at 150 K. Data for compound **7** were collected using an XtaLAB Synergy, Dualflex, HyPix-Arc 100 diffractometer with MoKα radiation at 150 K and 290 K. All data were processed with the CrysAlisPro software suite [39]. Analytical absorption correction was applied to all data sets. Structures were solved using the dual-space algorithm in SHELXT [40], implemented in the Olex2 crystallographic software [41]. Independent atom model (IAM) refinements were performed with the SHELXL-2019/3 software [42]. Hydrogen atoms on carbon atoms were placed at calculated positions and refined as riding atoms with isotropic displacement parameters. Hydrogen atoms on nitrogen and oxygen atoms were located using a difference Fourier map, and their positional parameters were refined freely. The structure of compound **1** is an example of a racemic twin, with the molar fraction of the second domain being 0.26(4).

After classical refinement using the IAM, Hirshfeld Atom Refinement (HAR) with the NoSpherA2 algorithm [43], as implemented in the Olex2 package, was performed for further refinement. For the non-spherical refinement, ORCA 6.0 was used [44]. The

predefined test options (basis set: 3–21 G; method: r2SCAN; integration accuracy: low) for the first cycle of non-spherical-atom refinement were applied, with the only modification being the change in the solvation setting from vacuum to water. The multiplicities were assigned according to the formula of the displayed fragment.

After the initial non-spherical refinement cycle, the positions and displacement parameters of the hydrogen atoms in the structures were first refined freely using the following sequence of commands to improve the models: refineHdist, affix 0, free uiso, and finally anis -h. All these commands were applied exclusively to all hydrogen atoms in the structure. For some structures, anisotropic refinement of hydrogen atoms (anis -h) did not significantly improve the model without strong constraints and was therefore omitted. Where necessary, constraints were applied to ensure that parameter shifts converged to zero. Improved non-spherical atomic scattering factors were then calculated with NoSpherA2, using the predefined Work (basis set: def2-SVP; method: r2SCAN; integration accuracy: low) and Final (basis set: def2-TZVP; method: r2SCAN; integration accuracy: normal; iterative mode) settings, except that the solvation model was changed from vacuum to water. Figures representing deformation maps were also created using Olex2. Thermal ellipsoids in all images are drawn at 50% probability.

Further details regarding the refinement procedure for each structure are provided in the Supplementary Materials (Table S9).

### *3.5. Creating Figures of Structures* **1–7**

Figures showing various features of the structures were created using Olex2 [41]. Thermal ellipsoids in all images are drawn at 50% probability.

### *3.6. Data Search in the Cambridge Structural Database (CSD)*

Neutron data for *Dabco* molecules were obtained from the CSD (Loganholme, Australia) using ConQuest software (version 6.01, November 2025) [45,46]. The search criteria were as follows:

- *Draw (the structural formula of the Dabco molecule was drawn);*
- *Experimental (neutron source selected).*

This initial search yielded 25 entries from the CSD, of which 8 were selected; the remainder were excluded from further analysis due to disorder of the *Dabco* molecule in the structure. To obtain C–H and N–H bond distances, two separate searches were conducted using the *add 3D* option in the Draw dialogue. Distances were then exported and analysed using Mercury software. The list of refcodes for the data sets used in the analysis is provided in the Supplementary Materials (Tables S3 and S4).

### *3.7. Powder X-Ray Data Collection*

The phase composition of the powder samples was determined by X-ray diffraction using a Bruker AXS D4 Endeavor diffractometer with Cu Kα radiation (λ = 1.5406 Å) and a Sol-X energy-dispersive detector, within the 2θ range from 5° to 60°, with a step size of 0.04° and a collection time of 6 s. Powder data were analysed and figures prepared using Match! software (version 4.1) [47].

### *3.8. Magnetic Measurements*

The magnetic properties of polycrystalline complexes **2**, **4** and **7** were measured using a Quantum Design MPMS3 SQUID magnetometer over the temperature range 2–300 K under a constant magnetic field of 1 kOe. Isothermal magnetisation was recorded at 2 K in the field range −50 kOe to 50 kOe. The raw data were corrected for the temperature-

independent diamagnetic contributions of the sample holder and the inner-shell electrons using Pascall's constants [48].

## 4. Conclusions

We have shown that crystallographic models can be improved by using NoSpherA2, a non-spherical structure refinement tool within Olex2, even when high-resolution data are unavailable (e.g., data collected with CuK$\alpha$). When using NoSpherA2, the C–H and N–H bond distances are closer to those obtained from neutron diffraction data than with classical refinement.

The study of the magnetic properties of compounds **2**, **4**, and **7** has shown that magnetic interactions between mononuclear copper(II) complexes are governed primarily by the bonding pathways between copper magnetic centres, rather than by the copper–copper distances. Despite similar copper–copper distances, compounds **2** and **4** display only weak antiferromagnetic properties, whereas compound **7** exhibits significantly stronger coupling upon cooling below 150 K, due to the presence of N–H···Br hydrogen bonds, in which the more diffuse and polarisable $Br^-$ orbitals provide an efficient magnetic exchange pathway. Notably, the presence of N–H···N hydrogen bonds alone in mononuclear copper(II) compounds does not necessarily lead to magnetic interactions, as demonstrated by compound **2**. Although N–H···N-mediated exchange pathways have been reported in the literature, the present results indicate that additional structural and electronic factors are required for efficient magnetic coupling. The absence of measurable exchange mediated solely by the bridging *μ-Dabco* ligand in compound **4** further indicates that this ligand acts primarily as a structural spacer rather than an efficient magnetic bridge. Compounds **2** and **4**, which lack N–H···Br bonds and have similar intermolecular copper–copper distances to compound **7**, exhibit antiferromagnetic properties only below 30 K. Moreover, the similarity of intra- and interchain Cu···Cu distances in the quasi-1D system prevents low-dimensional magnetic behaviour, emphasising the importance of using a 3D framework model.

**Supplementary Materials:** The following supporting information can be downloaded at: https://www.mdpi.com/article/10.3390/inorganics14020054/s1, Figure S1: Comparison of simulated (red) and measured (blue) powder patterns for compound **2**; Figure S2: Comparison of simulated (red) and measured (blue) powder patterns for compound **4**; Figure S3: Comparison of simulated (red) and measured (blue) powder patterns for compound **7**; Table S1: Table of crystalographic data after classical refinement for compounds **1**–**3**; Table S2: Table of crystalographic data after classical refinement for compounds **4**–**7**; Table S3: Table of the CSD refcodes and C-H bond distances in *Dabco* molecules from neutron diffraction experiments; Table S4: Table of the CSD refcodes and N-H bond distances in *Dabco* molecules from neutron diffraction experiments; Table S5: N-H bond distances in *Dabco* molecules of compounds **1**, **2**, **3**, **5** and **7** after classical refinement (IAM model). Compounds **4** and **6** do not contain *Dabco* molecules; Table S6: Table of C-H and N-H distances of *Dabco* molecules in structures **1**–**3** after non-spherical refinement (HAR model); Table S7: Table of C-H and N-H distances of *Dabco* molecules in structures **4**–**6** after non-spherical refinement (HAR model); Table S8: Table of C-H and N-H distances of *Dabco* molecules in structure **7** after non-spherical refinement (HAR model); Table S9: Table of NoSpherA2 commends and restrains used on refinement of different structures.

**Author Contributions:** Conceptualization, Ž.Z. and E.G.; methodology, Ž.Z., E.G. and Z.J.; validation, Ž.Z., E.G., Z.J. and S.Š.; formal analysis, Ž.Z., E.G. and Z.J.; investigation, Ž.Z., E.G., Z.J. and S.Š.; resources, Ž.Z., E.G., Z.J. and S.Š.; data curation, Ž.Z., E.G., Z.J. and S.Š.; writing—original draft preparation, Ž.Z., E.G., Z.J. and S.Š.; writing—review and editing, Ž.Z., E.G., Z.J. and S.Š.; visualization, Ž.Z. and Z.J.; supervision, E.G.; project administration, E.G.; funding acquisition, E.G., Z.J. and S.Š. All authors have read and agreed to the published version of the manuscript.

**Funding:** This research was funded by the Slovenian Research and Innovation Agency (research core funding No. P1–0045; Inorganic Chemistry and Technology; grant Nos. P2-0348 and J1-3026).

**Data Availability Statement:** CCDC 2346839, 2335461, 2335468, 2492241, 2332611, 2335469, 2517663 and 2517664 contain the supplementary crystallographic data for this paper. These data can be obtained free of charge via https://www.ccdc.cam.ac.uk/structures/ (accessed on 7 February 2026) (or from the CCDC, 12 Union Road, Cambridge CB2 1EZ, UK; Fax: +44 1223 336033; E-mail: deposit@ccdc.cam.ac.uk).

**Conflicts of Interest:** The authors declare no conflicts of interest. The funders had no role in the design of this study; in the collection, analyses, or interpretation of data; in the writing of this manuscript; or in the decision to publish the results.

## Abbreviations

The following abbreviations are used in this manuscript:

| | |
|---|---|
| ACN | acetonitrile |
| CSD | Cambridge Structural Database |
| *Dabco* | 1,4-diazabicyclo[2.2.2]octane |
| HAR | Hirshfeld atom refinement |
| H*Dabco* | Monoprotonated 1,4-diazabicyclo[2.2.2]octane |
| IAM | Independent Atom Model |
| MeOH | Methanol |

## References

1. Gusev, A.N.; Nemec, I.; Herchel, R.; Bayjyyev, E.; Nyshchimenko, G.A.; Alexandrov, G.G.; Eremenko, I.L.; Trávníček, Z.; Hasegawa, M.; Linert, W. Versatile coordination modes of bis[5-(2-pyridine-2-yl)-1,2,4-triazole-3-yl]alkanes in Cu(II) complexes. *Dalton Trans.* **2014**, *43*, 7153–7165. [CrossRef] [PubMed]
2. Yusuf, T.L.; Oladipo, S.D.; Zamisa, S.; Kumalo, H.M.; Lawal, I.A.; Lawal, M.M.; Mabuba, N. Design of New Schiff-Base Copper(II) Complexes: Synthesis, Crystal Structures, DFT Study, and Binding Potency toward Cytochrome P450 3A4. *ACS Omega* **2021**, *6*, 13704–13718. [CrossRef] [PubMed]
3. Golobič, A.; Kristl, M.; Podnar, T.M.; Jagličić, Z.; Dojer, B. Mixed-Ligand Copper(II) Complexes Derived from Pyridinecarbonitrile Precursors: Structural Features and Thermal Behavior. *Inorganics* **2025**, *13*, 287. [CrossRef]
4. Fomenko, I.S.; Afewerki, M.; Gongola, M.I.; Vasilyev, E.S.; Shul'pina, L.S.; Ikonnikov, N.S.; Shul'pin, G.B.; Samsonenko, D.G.; Yanshole, V.V.; Nadolinny, V.A.; et al. Novel Copper(II) Complexes with Dipinodiazafluorene Ligands: Synthesis, Structure, Magnetic and Catalytic Properties. *Molecules* **2022**, *27*, 4072. [CrossRef]
5. Baran, P.; Boča, R.; Breza, M.; Elias, H.; Fuess, H.; Jorík, V.; Klement, R.; Svoboda, I. The spectroscopic and structural properties of copper(II) complexes of the novel tridentate (ONO) pyridine N-oxide ligand Hpoxap. *Polyhedron* **2002**, *21*, 1561–1571. [CrossRef]
6. Spodine, E.; Atria, A.M.; Valenzuela, J.; Jalocha, J.; Manzur, J.; García, A.M.; Garland, M.T.; Peña, O.; Saillard, J.-Y. Magnetic properties of dinuclear copper(II) complexes with simple pyrazolate bridges. *J. Chem. Soc. Dalton Trans.* **1999**, 3029–3034. [CrossRef]
7. Petrenko, Y.P.; Khomenko, D.M.; Doroshchuk, R.O.; Shova, S.; Novitchi, G.; Piasta, K.; Gumienna-Kontecka, E.; Lampeka, R.D. Synthesis, crystal structure and magnetic properties of new copper(II) complexes based on 3-(2-pyridyl)-1,2,4-triazole. *Inorganica Chim. Acta* **2020**, *500*, 119216. [CrossRef]
8. Liu, J.C.; Fu, D.G.; Zhuang, J.Z.; Duan, C.Y.; You, X.Z. Linear trinuclear and one-dimensional copper(II) complexes containing co-bridging end-on azido and triazole ligands. Crystal structures and magnetic properties of $[Cu_3(atrz)_2(N_3)_6]$ and $[Cu(atrz)_2(N_3)]NO_3$ (atrz = 4-amino-1,2,4-triazole). *J. Chem. Soc. Dalton Trans.* **1999**, 2337–2342. [CrossRef]
9. Grove, H.; Julve, M.; Lloret, F.; Kruger, P.E.; Törnroos, K.W.; Sletten, J. Syntheses, crystal structures and magnetic properties of copper(II) polynuclear and dinuclear compounds with 2,3-bis(2-pyridyl)pyrazine (dpp) and pseudohalide as ligands. *Inorganica Chim. Acta* **2001**, *325*, 115–124. [CrossRef]
10. Silva, C.P.; Junior, H.C.; Santos, I.F.; Bernardino, A.M.; Cassaro, R.A.; Novak, M.A.; Vaz, M.G.; Guedes, G.P. Synthesis, crystal structure, magnetic properties and DFT calculations of a mononuclear copper(II) complex: Relevance of halogen bonding for magnetic interaction. *Inorganica Chim. Acta* **2018**, *482*, 395–401. [CrossRef]
11. Guedes, G.P.; Farias, F.F.; Novak, M.A.; MacHado, F.L.D.A.; Vaz, M.G.F. Synthesis, crystal structure, magnetism and specific heat of a new copper(II) compound with p-aminobenzoic acid. *Inorganica Chim. Acta* **2011**, *378*, 134–139. [CrossRef]
12. Santos, I.F.; Guedes, G.P.; Mercante, L.A.; Bernardino, A.M.R.; Vaz, M.G.F. Synthesis, crystal structure and magnetism of three novel copper(II) complexes with pyrazole-based ligands. *J. Mol. Struct.* **2012**, *1011*, 99–104. [CrossRef]

13. Willett, R.D.; Galeriu, C.; Landee, C.P.; Turnbull, M.M.; Twamley, B. Structure and Magnetism of a Spin Ladder System: $(C_5H_9NH_3)_2CuBr_4$. *Inorg. Chem.* **2004**, *43*, 3804–3811. [CrossRef] [PubMed]
14. Bedford, C.P.; Landee, C.P.; Wikaira, J.L.; Turnbull, M.M. Copper(II) halide salts of 5-bromo-2-aminopyridine and 3,5-dibromo-2-aminopyridine: Syntheses, structures and magnetic behavior. *J. Coord. Chem.* **2023**, *76*, 1353–1369. [CrossRef]
15. Awwadi, F.; Willett, R.D.; Twamley, B.; Schneider, R.; Landee, C.P. Strong Rail Spin 1/2 Antiferromagnetic Ladder Systems: (Dimethylammonium)(3,5-Dimethylpyridinium)$CuX_4$, X = Cl, Br. *Inorg. Chem.* **2008**, *47*, 9327–9332. [CrossRef] [PubMed]
16. Bertrand, J.A.; Black, T.D.; Eller, P.G.; Helm, F.T.; Mahmood, R. Polynuclear complexes with hydrogen-bonded bridges. Dinuclear complex of N,N′-bis(2-hydroxyethyl)-2,4-pentanediimine with copper(II). *Inorg. Chem.* **1976**, *15*, 2965–2970. [CrossRef]
17. Talukder, P.; Sen, S.; Mitra, S.; Dahlenberg, L.; Desplanches, C.; Sutter, J. Evidence for Hydrogen-Bond-Mediated Exchange Coupling in an Aqua-Bridged $Cu^{II}$ Dimer: Synthesis, Magnetic Study and Correlation with Density Functional Calculations. *Eur. J. Inorg. Chem.* **2006**, *2006*, 329–333. [CrossRef]
18. Haddad, S.F.; Willett, R.D.; Landee, C.P. Crystal structure and magnetic properties of $[C_6H_4(CH_2NH_3)_2][CuCl_3(H_2O)]Cl{\cdot}H_2O$. *Inorganica Chim. Acta* **2001**, *316*, 94–98. [CrossRef]
19. Luque, A.; Sertucha, J.; Lezama, L.; Rojo, T.; Róman, P. Synthesis, characterisation and crystal structure of 2-aminopyridinium(2-amino-5-bromopyridine)tribromocuprate(II) and bis(2-aminopyridinium)tetrabromocuprate(II). *J. Chem. Soc. Dalton Trans.* **1997**, 847–854. [CrossRef]
20. Levchenkov, S.I.; Shcherbakov, I.N.; Popov, L.D.; Lukov, V.V.; Minin, V.V.; Starikova, Z.A.; Ivannikova, E.V.; Tsaturyan, A.A.; Kogan, V.A. The magnetic exchange interaction via N–H···O-bonding in copper(II) complex with 1-phenyl-3-methyl-4-formylpyrazol-5-one 2-quinolylhydrazone. *Inorganica Chim. Acta* **2013**, *405*, 169–175. [CrossRef]
21. Florencio, A.S.; Allão, R.A.; Vaz, M.G.F.; Carneiro, J.W.D.M. Density Functional Theory as a tool to identify the dominant magnetic interactions in the $[Cu(hfac)_2(N_3TEMPO)]_n$ chain. *Inorg. Chem. Commun.* **2012**, *24*, 67–69. [CrossRef]
22. Desplanches, C.; Ruiz, E.; Rodríguez-Fortea, A.; Alvarez, S. Exchange Coupling of Transition-Metal Ions through Hydrogen Bonding: A Theoretical Investigation. *J. Am. Chem. Soc.* **2002**, *124*, 5197–5205. [CrossRef] [PubMed]
23. Bader, K.; Dengler, D.; Lenz, S.; Endeward, B.; Jiang, S.-D.; Neugebauer, P.; van Slageren, J. Room temperature quantum coherence in a potential molecular qubit. *Nat. Commun.* **2014**, *5*, 5304. [CrossRef] [PubMed]
24. Vakulka, A.; Goreshnik, E. Copper(I) bromide and chloride complexes with urotropine and triethylenediamine: Synthesis, crystal structure, and Raman characterization. *J. Coord. Chem.* **2018**, *71*, 2426–2440. [CrossRef]
25. Luo, X.; Cao, Y.; Wang, T.; Li, G.; Li, J.; Yang, Y.; Xu, Z.; Zhang, J.; Huo, Q.; Liu, Y.; et al. Host–Guest Chirality Interplay: A Mutually Induced Formation of a Chiral ZMOF and Its Double-Helix Polymer Guests. *J. Am. Chem. Soc.* **2016**, *138*, 786–789. [CrossRef]
26. Braga, D.; Maini, L.; Mazzeo, P.P.; Ventura, B. Reversible Interconversion between Luminescent Isomeric Metal–Organic Frameworks of $[Cu_4I_4(DABCO)_2]$ (DABCO=1,4-Diazabicyclo[2.2.2]octane). *Chem.—A Eur. J.* **2010**, *16*, 1553–1559. [CrossRef]
27. Armelao, L.; Rando, M.; Carlotto, S.; Motta, I.; Bottaro, G.; Rancan, M. Bridging two worlds: (DABCO-H)$CuKI_3$ a hybrid copper iodide phosphor with a perovskite structure. *Pure Appl. Chem.* **2024**, *96*, 69–80. [CrossRef]
28. Zhu, K.; Reid, O.; Rangan, S.; Wang, L.; Li, J.; Durai, K.A.J.; Zhou, K.; Javed, N.; Kasaei, L.; Yang, C.; et al. Dual interfacial H-bonding-enhanced deep-blue hybrid copper–iodide LEDs. *Nature* **2025**, *643*, 1246–1254. [CrossRef]
29. Yue, C.-Y.; Lin, N.; Gao, L.; Jin, Y.-X.; Liu, Z.-Y.; Cao, Y.-Y.; Han, S.-S.; Lian, X.-K.; Hu, B.; Lei, X.-W. Organic cation directed one-dimensional cuprous halide compounds: Syntheses, crystal structures and photoluminescence properties. *Dalton Trans.* **2019**, *48*, 10151–10159. [CrossRef]
30. Tian, D.; Xu, H.; Yang, L.-O.; Zhou, J.; Lin, F.; Liu, X.; Tan, K.; Xie, R.-J.; Chen, X. Tunable Emission of Low-Dimensional Organic Metal Halides by Stoichiometric Ratio and Metal Center. *Inorg. Chem.* **2024**, *63*, 4738–4746. [CrossRef]
31. Goreshnik, E. Influence of the synthetic conditions on a formation of 1-D, 2-D and 3-D copper–chloride coordination polymers. *CrystEngComm* **2021**, *23*, 7171–7178. [CrossRef]
32. Zhang, Y.; Wang, B. 1,4-Diazoniabicyclo[2.2.2]octane tetrabromidocuprate(II) monohydrate. *Acta Crystallogr. Sect. E Struct. Rep. Online* **2011**, *67*, m371. [CrossRef] [PubMed]
33. Addison, A.W.; Rao, T.N.; Reedijk, J.; van Rijn, J.; Verschoor, G.C. Synthesis, structure, and spectroscopic properties of copper(II) compounds containing nitrogen–sulphur donor ligands; the crystal and molecular structure of aqua[1,7-bis(N-methylbenzimidazol-2′-yl)-2,6-dithiaheptane]copper(II) perchlorate. *J. Chem. Soc. Dalton Trans.* **1984**, 1349–1356. [CrossRef]
34. Alvarez, S. A cartography of the van der Waals territories. *Dalton Trans.* **2013**, *42*, 8617–8636. [CrossRef]
35. Slater, J.C. Atomic Radii in Crystals. *J. Chem. Phys.* **1964**, *41*, 3199–3204. [CrossRef]
36. Yang, L.; Powell, D.R.; Houser, R.P. Structural variation in copper(i) complexes with pyridylmethylamide ligands: Structural analysis with a new four-coordinate geometry index, $\tau_4$. *Dalton Trans.* **2007**, 955–964. [CrossRef]
37. Ashcroft, N.W.; Mermin, N.D. *Solid State Physics*; Harcourt Brace: San Diego, CA, USA, 1976.
38. Chilton, N.F.; Anderson, R.P.; Turner, L.D.; Soncini, A.; Murray, K.S. PHI: A powerful new program for the analysis of anisotropic monomeric and exchange-coupled polynuclear *d*- and *f*-block complexes. *J. Comput. Chem.* **2013**, *34*, 1164–1175. [CrossRef]

39. Diffraction, R.O. *CrysAlisPRO*; Yarnton: Oxfordshire, UK, 2024.
40. Sheldrick, G.M. *SHELXT*—Integrated space-group and crystal-structure determination. *Acta Crystallogr. Sect. A Found. Adv.* **2015**, *71*, 3–8. [CrossRef]
41. Dolomanov, O.V.; Bourhis, L.J.; Gildea, R.J.; Howard, J.A.K.; Puschmann, H. *OLEX2*: A complete structure solution, refinement and analysis program. *J. Appl. Crystallogr.* **2009**, *42*, 339–341. [CrossRef]
42. Sheldrick, G.M. Crystal structure refinement with *SHELXL*. *Acta Crystallogr. Sect. C Struct. Chem.* **2015**, *71*, 3–8. [CrossRef]
43. Kleemiss, F.; Dolomanov, O.V.; Bodensteiner, M.; Peyerimhoff, N.; Midgley, L.; Bourhis, L.J.; Genoni, A.; Malaspina, L.A.; Jayatilaka, D.; Spencer, J.L.; et al. Accurate crystal structures and chemical properties from NoSpherA2. *Chem. Sci.* **2021**, *12*, 1675–1692. [CrossRef]
44. Neese, F. Software Update: The *ORCA* Program System—Version 6.0. *WIREs Comput. Mol. Sci.* **2025**, *15*, e70019. [CrossRef]
45. Groom, C.R.; Bruno, I.J.; Lightfoot, M.P.; Ward, S.C. The Cambridge Structural Database. *Struct. Sci. Cryst. Eng. Mater.* **2016**, *72*, 171–179. [CrossRef]
46. Bruno, I.J.; Cole, J.C.; Edgington, P.R.; Kessler, M.; Macrae, C.F.; McCabe, P.; Pearson, J.; Taylor, R. New software for searching the Cambridge Structural Database and visualizing crystal structures. *Struct. Sci. Cryst. Eng. Mater.* **2002**, *58*, 389–397. [CrossRef]
47. Putz, H.; Brandenburg, K. Match!—Phase Analysis using Powder Diffraction, Crystal Impact. *GbR Kreuzherrenstr* **2003**, *102*, 53227.
48. Bain, G.A.; Berry, J.F. Diamagnetic Corrections and Pascal's Constants. *J. Chem. Educ.* **2008**, *85*, 532–536. [CrossRef]